Influence of displacement piles on surrounding soil and nearby piles: a case study

Hendrik Jan Tuenter, Virginia Herrera, Victor Rozalén [i)], David Leuenberger [ii)]

i) Geoprofile GmbH, beratende Ingenieure, Ebikonerstrasse 75, CH-6043 Adligenswil, Switzerland

ii) Marti Gründungstechnik AG, Lochackerweg 2, CH-3302 Moosseedorf, Switzerland

ABSTRACT

For a large construction project in the greater Zug area (Switzerland), four maintained load axial pile loading test were performed on 600 und 700 mm diameter, 45 m long full displacement piles. The maximum test load was around 7800 kN. All test pile rebar cages were fitted with fiber-optic distributed sensing temperature and strain sensors, allowing thermal integrity profiling of the test piles and the measurement of residual load. Because of the large pile diameter and nearby sensitive infrastructure, pile installation was accompanied by a comprehensive monitoring of free field soil displacement and heave. Pile installation monitoring comprised ten purpose built push in soil extensometers to measure vertical soil heave at various depths, total station measurements and precision levelling for measuring surface displacement and heave, and measurement of excess pore water pressures during installation. The results of heave and lateral displacements are accordingly calculated by Cavity Expansion (CE) and Shallow Strain Path Method (SSPM) and modifying factors are recommended to improve predictions with SSPM that can take into account soil compressibility for non-homogeneous, layered soils.

Keywords: full displacement pile, static pile load test, soil displacement, soil heave, shallow strain path method, residual load

1 INTRODUCTION

The use of cast-in-place full displacement piles is common in Switzerland. The envelope for the application of such piles has extended continuously, as longer piles with larger diameters have become commercially available. Taking advantage of recent technological advances, the construction of a new office complex in the greater Zug area in central Switzerland called for the installation of over 800 high capacity cast-in-place full displacement piles with a proposed length of 45 m. The design value for the pile load E_d was in the order of 4000 kN. In view of the high pile loads and large number of piles, final design called for the execution of four maintained load axial pile loading test. All test piles were fitted with fiber-optic distributed sensing temperature and strain sensors to establish the pile shape and the load transfer with depth.

However, the proposed pile diameter and the sheer number of piles also implies a large volume of displaced soil. This exacerbates potential problems associated with lateral soil displacements and soil heave. Difficulties associated with soil movement include its effects on nearby buildings and infrastructure, and problems associated with pile integrity for piles already constructed. In particular, tensile stresses may develop in the pile shaft, and pile uplift may occur. These tensile stresses transition into compressive stresses after soil settlement only (residual force).

State-of-the-art practice regarding lateral soil displacement and soil heave typically assumes undrained soil conditions. Comprehensive methodologies to assess these effects in layered, non-homogenous or compressible soils are scarce. With the objective to quantify soil displacements in these sort of 'real world' soils, a comprehensive monitoring program of free field soil displacement and heave accompanied the installation of the test and reaction piles.

THEORETICAL CONSIDERATIONS

Hagerty and Peck (1971) found that the volume of displaced soil is essentially equal to the volume of the inserted pile. At depths of penetration greater than about

ten times the radius of the pile, the soil is primarily displaced laterally (Cooke and Price 1973). Assuming an isotropic undrained medium, the soil is displaced in concentric circles. The circle width decreases as the circumference increases away from the pile (figure 1).

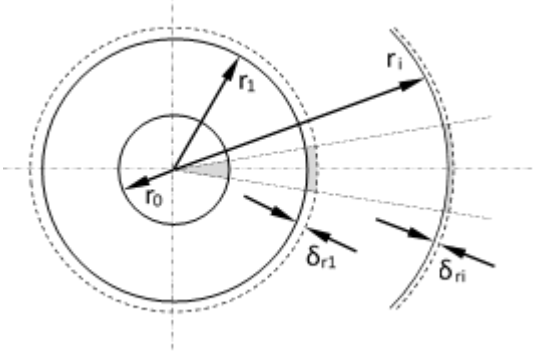

Fig. 1. Cylindrical cavity expansion in an incompressible medium. The grey shading denotes areas of similar surface area.

Assuming purely cylindrical cavity expansion, the lateral displacement δ_r can be described as follows (Chong, 2001):

$$\frac{\delta_r}{r_0} = \frac{r_0}{2r} \tag{1}$$

with r_0 denoting the radius of the pile and r the radial distance from the pile center. Randolph et al. (1979) performed laboratory chamber tests to evaluate the effects of pile penetration in clays. Their results and those from other researchers (Cooke and Price 1973; Carter et al. 1979; Ni et al,. 2010) indicate that the lateral ground displacement δ_r due to pile driving can be approximated by the lateral displacement due to the expansion of a cylindrical cavity with radius equal to the pile radius:

$$\frac{\delta_r}{r_0} = \left[\left(\frac{r}{r_0}\right)^2 + 1\right] - \frac{r}{r_0} \tag{2}$$

This solution is essentially equivalent to (1). At a distance of 3 times the pile radius, the difference is 2.6 percent and approaching zero at larger distances. The shallow strain path method (SSPM), using an adapted strain path method to include the effects of a free ground surface using corrective shear stresses, can be written in similar terms as [1] (Baligh, 1985; Sagaseta et al., 1997; Sagaseta and Whittle, 2001):

$$\frac{\delta_r}{r_0} = \frac{r_0}{2r} \cdot \frac{L}{\sqrt{r^2+L^2}} \tag{3}$$

where L denotes the pile length. It is clear that for long and slender piles, this solution approaches cylindrical cavity conditions (1).

With regard to vertical displacement with depth and at the ground surface (heave), Poulos (1994) provides an approximate solution using the strain path method. Sagaseta et al. (1997) provide a theoretical framework, but a closed form solution only exists at the ground surface:

$$\delta_{z,0} = -\frac{r_0}{2} \cdot \left(\frac{1}{r} - \frac{1}{\sqrt{r^2+L^2}}\right) \tag{4}$$

Chong (2013), using considerations of strain energy and work done, derives a heave function f_v, describing the vertical heave at ground surface as a fraction of the lateral displacements:

$$\delta_{z,0} = f_v \cdot \delta_r \tag{5}$$

Theoretical solutions may overpredict lateral displacement (Ni and Guymer, 2010). Solutions assuming cylindrical cavity expansion ignore the soil volume "lost" to heave and hence not displaced laterally. Acknowledging this, Chong (2013) introduced a correction factor b to (1) of the form

$$\frac{\delta_r}{r_0} = \frac{r_0}{2r} e^{-br} \tag{6}$$

Note that Chong (2013) provides a methodology for deriving b, which requires the calculation of a heave function f_v, denoting the ratio of vertical to lateral displacement at any given point. The analytical calculation of this heave function is relatively complex and not reproduced here; for details the original publication refers.

2 GEOLOGICAL SETTING

The building site is located in Baar, part of the greater Zug area in central Switzerland. The depositional sequence essentially results from the late Pleistocene and Holocene filling of the northern Lake Zug basin ("Baarer Becken").

Up until a depth of 5 m, the soil consists of recent fine-grained overbank deposits, containing significant amounts of organic material. Immediately below follow fluvial sands, containing some gravel. From about 9 m onward follows a large sequence of interbedded sands and silts, transitioning into primarily fine-grained lake deposits containing frequent sand layers and debris deposited by melting icebergs floating on the periglacial lake (e. g. drop stones). Figure 2 shows data from the cone penetration test performed in the immediate vicinity of the test piles. A 0.6 m thick gravel working platform was placed at the surface prior to pile installation.

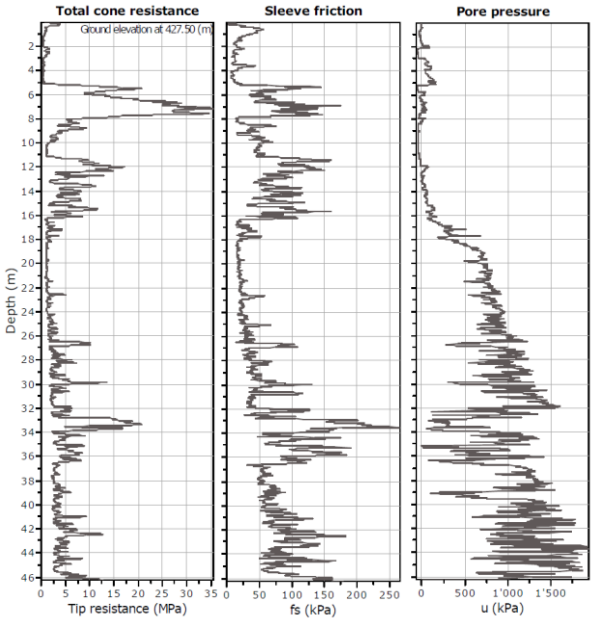

Fig. 2. Cone penetration test data

3 PILE DESIGN AND INSTALLATION

3.1 Preliminary design

Preliminary pile design considered the use of high capacity cast-in-place full displacement piles (Fundex type), the use of which is quite common in Switzerland. Technological advances have pushed the envelope of applicability, and commercially available pile lengths range up to 45 m with pile diameters of up to 700 mm.

Initial design considered the UniCone method (Niazi and Mayne, 2016; Eslami and Fellenius, 1997). However, as the original database used for this method does not include cast-in-place full displacement piles, the selected approach considered values of 1.45 for the shaft coefficient C_{se} (expected value) and 1.21 (characteristic value), respectively (Tuenter and Rozálen García, 2017). Assuming a C30/37 concrete, results showed that the internal resistance of the pile shaft at a characteristic level would be in the order of the external pile resistance. The load-displacement at the pile head considered a ratio function, using an exponent of 0.3 to describe the mobilization of the skin friction (t-z) and a value of 0.8 to describe the pile toe (Q-z), and considering elastic shortening. The neutral plane without any external load was calculated at 32.5 m. Figure 6a through 6d present results of the preliminary design.

3.2 Pile instrumentation and installation

The test setup considered two separate areas A and B. Test area A considered a nominal pile diameter of 600 mm, whereas for test area B a 700 mm nominal pile diameter was used. Prior to piling, each test pile was fitted with four Solifos glass fiber distributed temperature sensing cables located every 90 degrees around the rebar perimeter as well as two opposite Solifos BruSens v9 distributed strain sensing cables. In addition, each test pile was fitted with two Sisgeo vibrating wire embedded strain gauges and thermistors in the vicinity of the pile tip.

Pile installation started on March 22, 2021 and was completed 7 days later. The drill rig used was an IHC Fundex F3500 with an operational weight of 120 to and a maximum torque of 500 kNm, operated by an experienced drill crew. Rather than the standard cast iron Fundex sacrificial tip, a proprietary pile tip was used (sMartex Screw). A total of 8 reaction piles as well as 4 test piles were drilled down to 45 m. All reaction piles as well as test pile P1 and P2 had a nominal shaft diameter of 600 mm, whereas the nominal shaft diameter of test pile P3 and P4 was 700 mm. The average time required for drilling to target depth was about 15 minutes for the 600 mm diameter and around 20 minutes for the 700 mm diameter piles. Table 1 summarizes pile installation.

Table 1. Summary of pile installation.

pile nº.	construction order	construction date and time	pile type	diameter (mm)
P10	5	03-23-2021, 09:55	reaction pile	600
P11	1	03-22-2021, 10:05	reaction pile	600
P12	6	03-23-2021, 11:50	reaction pile	600
P13	2	03-22-2021, 13:20	reaction pile	600
P14	7	03-23-2021, 14:35	reaction pile	600
P15	3	03-22-2021, 15:40	reaction pile	600
P16	9	03-24-2021, 12:50	reaction pile	600
P17	4	03-23-2021, 07:35	reaction pile	600
P1	8	03-24-2021, 07:59	test pile	600
P2	10	03-25-2021, 07:50	test pile	600
P3	11	03-26-2021, 07:35	test pile	700
P4	12	03-29-2021, 07:30	test pile	700

The concrete used for casting showed a 28 days cubic compressive strength of around 42 MPa. The wet concrete included an admixture delaying the setting for about 4 hours. The concrete was cast after lowering the 45 m long 8x 18 rebar cage through the steel drill pipe using a concrete pump truck. After retraction of the drill pipe, the pile head was carefully constructed using a sacrificial 1 m long steel tube. In addition to the rebar cage, the upper 6 m of the pile shaft was reinforced using a centrally located HEB 160 S355 steel beam

All piles showed a visible outflow of groundwater at the pile head ("bleeding"), which continued for one to several hours, depending on the actual pile. The cumulative groundwater outflow was significant and in the order of a hundred liter per pile.

After completion of the test pile and cleansing of the immediate work area, the distributed temperature sensing cables were connected to a data logger. Temperature development during concrete curing along the distributed temperature sensing cables was monitored for all four test piles and subsequently converted to effective pile radius as per TIP method (Johnson, 2016). The results showed a more or less

homogeneous pile shaft of around 0.605 m and 0.705 m, respectively with a slight but clearly identifiable reduction in diameter of around 3.5 cm from about 36 m onward. TIP readings in the vicinity of the pile head (upper 2 to 3 m) were heavily influenced by the reduction of transient pore water pressures and the associated bleeding of the concrete observed at the pile head. Concrete curing in the upper 2 to 3 m was significantly slower in comparison to the rest of the piles and started with a delay of around 24 hours.

Unfortunately, on account of damage to a fiber-optic data logger connection port, baseline values for the strain immediately after concrete pouring could only be taken at test pile nr. 1; strain measurements for test piles 2 through 4 could only be zeroed before static loading.

3.3 Free field monitoring programme

A free-field monitoring programme complemented pile installation. The monitoring programme included 15 ground surface observation points located at variable distances and perpendicular to the axis of the test piles at test pile location P1 and P4, denoted line A and line B. The surface observation points were monitored using a Leica ICON iCR70 Robotic total station after the construction of every pile. In addition, the vertical level of each observation point was manually recorded after construction of every pile using a Leica DNA03 digital level.

Ten push-in and spring-tensioned fiber glass rod extensometers connected to a datalogger installed at two separate locations measured the soil heave in various depths. The extensometers were measured from a 6 m long reference beam, supported by heavy blocks resting on the ground surface on either end of the beam. The displacement was recorded every 15 minutes. The location and height of the beam support blocks and the ground surface measuring location below the reference beam were independently measured before and after the installation of a pile using the total station (xyz) and the digital level (z).

Two vibrating wire push-in pressure gauges installed at a depth of 20 m measured excess pore water pressure in 15 minute intervals. Table 2 and figures 4 and 5 show the setup of the monitoring programme.

Table 2. Distance from test pile to measuring points.

prism nº	distance to pile n°1 (m)	prism nº	distance to pile n°4 (m)
A1	1.0	B1	1.0
A2	2.1	B2	2.2
A3	5.1	B3	5.1
A4	7.5	B4	10.2
A5	10.1	B5	20.1
A6	20.0	B6	30.2
A7	29.9	B7	40.1
A8	40.0		

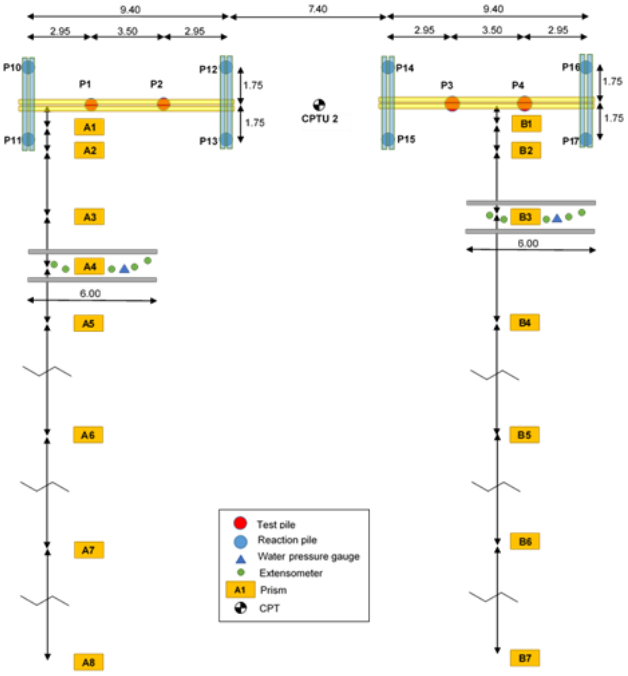

Fig. 3. Monitoring and static load test setup

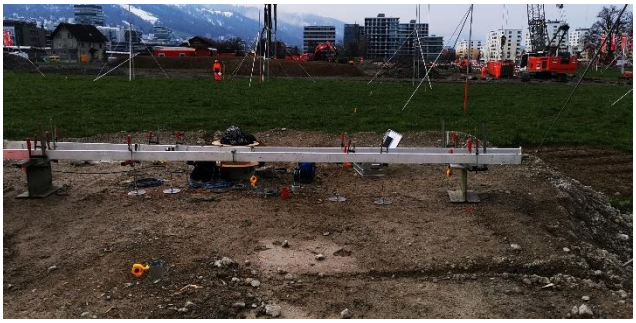

Fig. 4. Free field monitoring at location A4 in direction A8. Surface monitoring points (prisms), extensometer, porewater pressure sensor and reference beam are visible.

Fig. 5. Static pile load test with steel truss and reference beam

Operationally, the time window for installation of the instrumentation was limited to five days only. A further challenge was posed by a third party contractor working on site during pile installation (figure 4, background), introducing additional noise and requiring extensive coordination.

4 TEST EXECUTION AND RESULTS

4.1 Methodology

The test setup considered two separate areas, each with two test piles 3.5 m apart and in combination with four reaction piles. For each test area, a steel truss consisting of two steel HEM 1000 beams with additional reinforcement was installed, allowing the loading of two piles per test area without the need for moving the steel truss. Figure 2 details the test setup.

All tests were executed as maintained load tests as per Swiss code SN 505 267/1. The absolute displacements at the pile head were measured by three displacement transducers, mounted to a steel reference frame. Using a Leica DNA03 digital level located at a distance of 10 m from the piles, the elevation of the reference frame was periodically monitored. A constant pressure pump with Emerson ER3000 electronic controller regulated the pressure in the 800 to hydraulic jack and kept the load constant during each load step. The actual load output was measured using three 3000 kN load cells. The load steps were programmed prior to testing, whilst test control was remote via internet, allowing modification of the load programme if so required. Strain along the pile shaft was measured using an OZoptics ForeSight Brillouin Optical Time Domain Analyzer (BOTDA), using a 1ns pulse width (spatial resolution 0.1 m, discretization interval 0.04 m). Data was logged every 5 minutes. Strain measurements from the last 5 measurements during each load step were averaged and used for further analyses.

4.2 Results (static pile load test)

For the 600 mm diameter piles, the maximum applied load during testing as per load cell was around 6800 kN (hydraulic jack: 7000 kN). The maximum displacement of the pile head was slightly over 26 mm for both piles. For the 700 mm diameter piles, the maximum applied load during testing as per load cell was around 7750 kN (hydraulic jack: 7800 kN). The maximum displacement of the pile head was ca. 27 mm for P3 and around 37 mm for P4. The maximum load was limited due to safety concerns (Ø 600 mm) and the maximum force of the hydraulic jack (Ø 700 mm), respectively. Figure 6a through d present results for the displacement at the pile head.

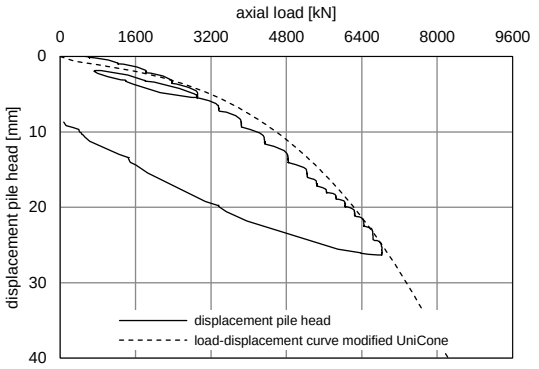

Fig. 6a. Load-displacement at pile head (P1, Ø 600 mm).

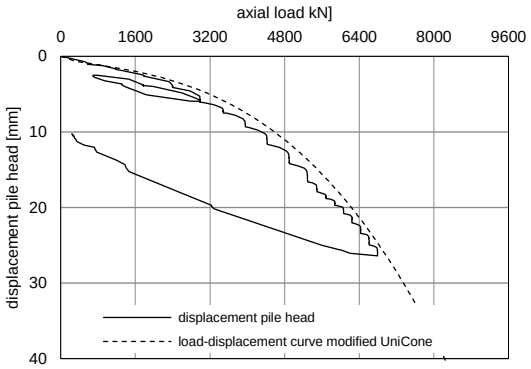

Fig. 6b. Load-displacement at pile head (P2, Ø 600 mm).

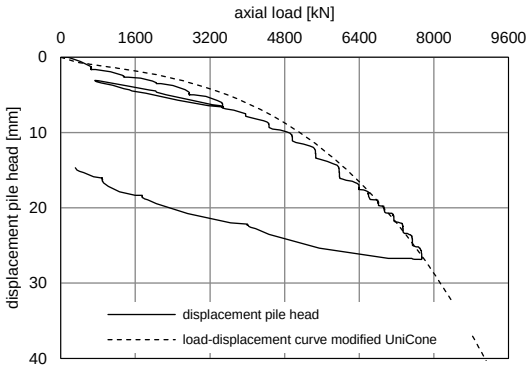

Fig. 6c. Load-displacement at pile head (P3, Ø 700 mm).

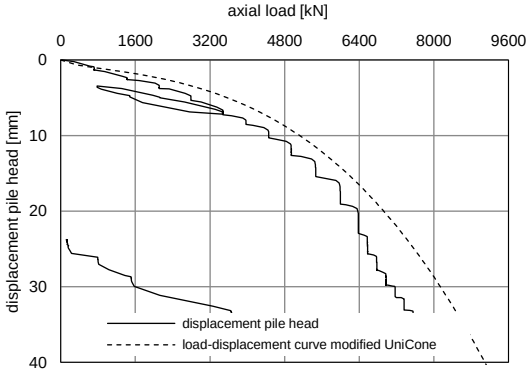

Fig. 6d. Load-displacement at pile head (P4, Ø 700 mm).

Figure 7a shows the strains present along the pile shaft P1 prior to loading, and during the highest load step. Strain measurements were zeroed immediately after concrete casting. Also shown are the strains along the pile shaft at the same load step, but zeroed prior to testing. Figure 7b shows the location of the neutral plane. For clarity, the strains have been converted to forces using the pile geometry derived from the TIP results and assuming a homogeneous elastic modulus of 30 GPa.

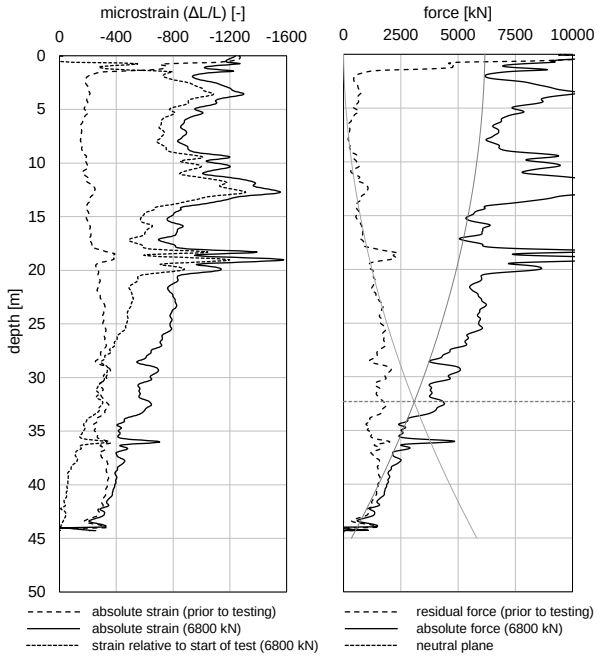

Fig. 7a and 7b. Residual strain, residual force and location of the neutral plane, constructed using the beta-method (β=0.3).

4.3 Results (field monitoring)

For reasons outlined earlier, the measurement of lateral soil displacement and heave at the surface show considerable levels of noise. During data processing, anomalous measurements were disregarded (e.g. unintended dislocation of observation points by construction workers or heavy machinery). In addition, field observations and construction logs were carefully scrutinized to ensure data integrity, resulting in the rejection of additional data points. Figures 8a and 8b show the measured displacement and heave of all high confidence data points. The data show a clear trend and decrease exponentially away from the pile axis.

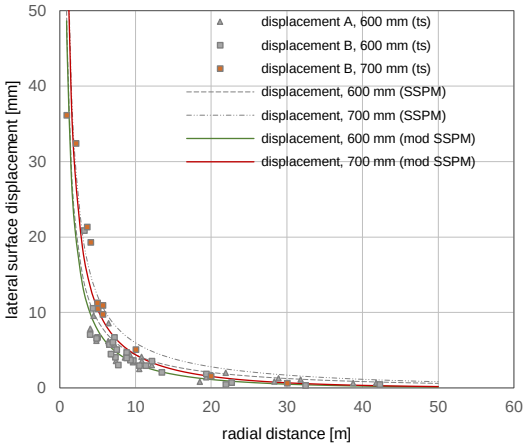

Fig. 8a. Measured lateral surface displacement for lines A and B. Dotted lines: SSPM prediction, continuous lines: modified SSPM. Note: ts denotes total station, dl denotes digital level.

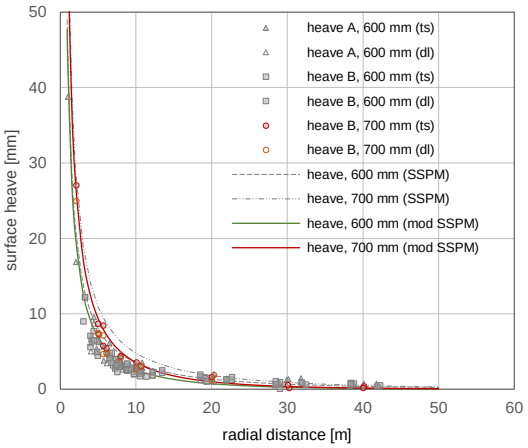

Fig. 8b. Measured surface heave for lines A and B. Continuous lines: SSPM prediction and modified SSPM. Note: ts denotes total station, dl denotes digital level.

Figures 9a though 9d show results for the pore water pressure and extensometer data, relative to the ground-supported reference beam as well as in absolute height relative to the start of piling. Data show an increase in the vertical displacement of the extensometers for each pile drilled, followed by a decrease in vertical displacement as the soil starts to resettle during periods of rest. Similarly, a sudden rise in pore water pressure is observed for each pile drilled within a radial distance of about 15 m of the pressure sensor, and a subsequent decrease in pressure during periods of rest (evening and night). The decrease in excess porewater pressure correlates with the resettling of the soil. Diurnal effects (changes in temperature and humidity) are visible as a time-limited pseudo-rise, in particular in line B. This is attributed to changes in temperature and humidity of the organic topsoil underlying the gravel working platform, leading to diurnal heave of the topsoil and hence the surface supported reference beam.

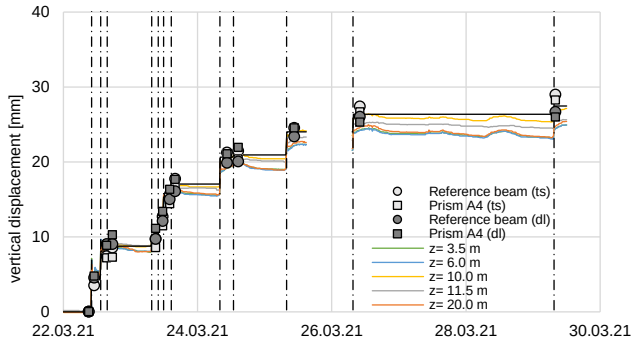

Fig. 9a. Measured vertical displacement of the reference beam and prism A4. Extensometer data of line A, in absolute height relative to the start of piling.

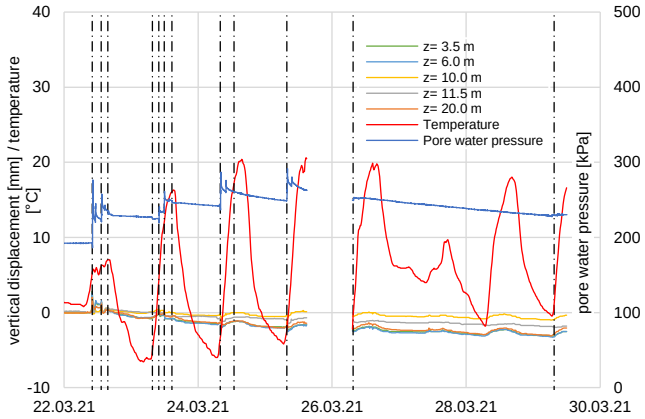

Fig. 9b. Extensometer data of line A, relative to the ground-supported reference beam. Measured pore water pressure and temperature

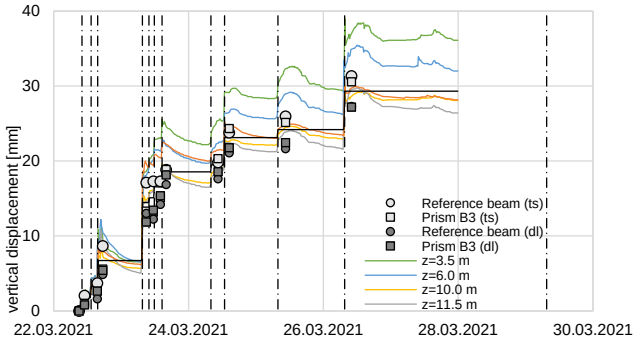

Fig. 9c. Measured vertical displacement of the reference beam and prism B3. Extensometer data of line B, relative to the ground-supported reference beam.

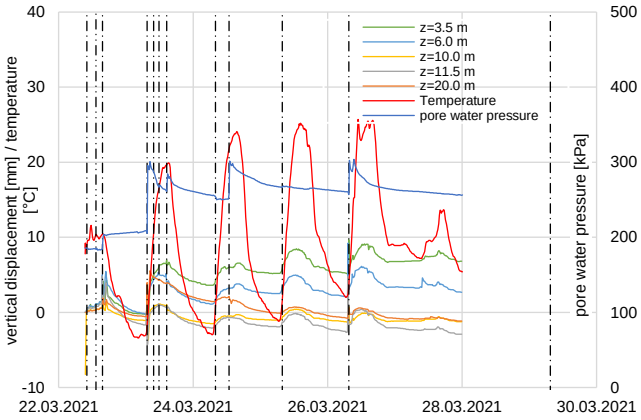

Fig. 9d. Extensometer data of line B, relative to the ground-supported reference beam. Measured pore water pressure and temperature

5 DISCUSSION

5.1 Static pile load test

Despite the high axial loads, none of the test piles reached their respective ultimate bearing resistance, neither per Eurocode nor per Swiss code. This is in line with results from the preliminary design. The predicted load-displacement curve correlate reasonably well with the measured load-displacement response at the pile head (figures 4a through d). Using a characteristic value of 1.21 for C_{se} would generally underpredict the stiffness of the test piles at higher loads, which follows from the definition of a characteristic value (likelihood of skin resistance being less than the characteristic value 5 percent). Pile no. 4 shows a more flexible pile head response. The resting period between pile construction and testing was around 15 days for all piles, suggesting that differences in skin friction buildup is probably not the cause. Concrete usage war essentially the same, and TIP records show a very similar pile shape. The centerline distance between P3 and P4 (3.5 m) is very small, rendering significantly different soil conditions highly unlikely. It is observed, however, that pile P4 was the last to be constructed. Pile P4 hence did not experience any upward vertical soil displacement caused by the construction of subsequent displacement piles. Indeed, the excess displacement of the pile head in comparison to P3 is about 10 mm (37 mm at the last load step vs. 27 mm for P3). This is the same order of magnitude as the average upward soil displacements expected along the pile shaft for P3 due to the construction of P4 and subsequent, partial reconsolidation.

Inspection of the absolute strain in pile P1 prior to testing shows that significant strains are already present in the pile shaft. The average strain rises from about 150 με at a depth of about 7 m and increases along pile shaft to over 300 με from 30 m onwards, before falling to about 200 με. During measurement of the strains prior to testing, no load was acting on the pile head. This

suggests that a certain amount of plastic and irreversible base strain is present along the entire pile shaft, together with an additional, variable component. The amount of base strain can be determined by converting the strains to forces using an appropriate choice for the elastic module E and the pile area A, and fitting a curve through the origin and the converted forces using the Beta-method (Fig. 7b). This method links the effective vertical stress to the skin friction using some fraction (β). The base strain is then determined iteratively by deducting a fixed amount of strain (assumed irreversible) from the measured strain until the Beta-method curve fits well. Using this procedure, the base strain is found to be in the order of 125 με This 'baseline' strain is irreversible and likely to be associated with the volume reduction during curing of the concrete. Using Bamforth et al. (2008), autogenous shrinkage due to curing of the concrete for the 14 day period between casting and testing is only around 35 με. The remainder (around 90 με) is believed to result from soil reconsolidation during the initial stages of concrete curing, during which the concrete strength is still less then the stresses introduced in the pile shaft. Again using Bamforth et al. (2008), this period is estimated to be in the order of 12 hours. Using a pile length of 45 m, the plastic shortening during this very early stage must be around 4 mm (i. e. 89 με). A first order estimate of the amount of soil reconsolidation in the immediate vicinity of pile P1 during the first 12 hrs considers the measured settlement of the extensometers at location A4 after the installation of pile P1 (ca. 0.5 mm). Noting that this location is 7.5 m away from the pile centre and that the ratio between the surface heave at a distance of 7.5 m and the immediate vicinity of the pile (taken as 1 m) is about 9, this implies an average soil reconsolidation of around 4.5 mm during the first 12 hours after casting. Considering that this strain is irreversible and does not relate to the forces in the pile, it should be excluded from any residual force analyses.

The variable, elastic strain component represents the effects of heave and soil reconsolidation, resulting in residual forces present along the pile shaft (Fellenius, 2022). The location of the neutral plane was established at 32.3 m, which correlates very well with the predicted 32.5 m from the preliminary design phase.

Absolute strains for P1 also show several distinct zones showing significantly higher level of absolute strain, in particular beween 18 and 20 m as well as around 36 m. Casting was by continuously pumping the plant-produced concrete mix, rendering excessive variability in the quality unlikely. The extraction of the drill pipe was realized immediately after concrete casting, with the (retarded) concrete still in the liquid state. Therefore, these zones most likely represent areas with significant microfissuring, not related to curing. These zones likely reflect the effects of soil heave and subsequent reconsolidation, introducing tensile and compressive stresses along the (young) pile shaft. Also visible are zones with an elevated strain level developing during the load test. These zones are restricted to the upper third of the pile and reflect the high levels of axial stress introduced.

5.2 Soil displacements

The results of the field monitoring programme show several features. First, the lateral displacements and soil heave caused by the displacement of the soil during pile installation are measured a significant distance away from the piles. The deformations appear to decrease exponentially. The SSPM method tends to slightly overpredict soil displacements. This reason for this is believed to be some degree of compressibility of the soils. To quantify these effects, equation (6) can be rewritten to a practically equivalent form as

$$\frac{\delta_r}{r_0} = \frac{r_0}{2r}(1-b)^r \qquad (7)$$

which illustrates that the correction factor b essentially denotes the fraction of soil per unit volume "lost", that is, not passed on laterally on account of heave, soil compressibility or some other reason. Noting that the SSPM solution for long, slender piles is essentially equivalent to (6), it is possible to modify equation (3) with the same damper function:

$$\frac{\delta_r}{r_0} = \frac{r_0}{2r} \cdot \frac{L}{\sqrt{r^2+L^2}} \cdot (1-b)^r \qquad (8)$$

The concept of the correction factor b is useful as it provides a practical means for extending the theoretical framework to compressible soils. For instance, for a loose sand it is well known that compaction takes place as a result of pile installation. Hence, a (large) percentage of the loose sand displaced would be "lost" due to compaction and would not be passed on any further. Compaction thus works as damper on the radial displacements. Few soils behave perfectly undrained, and the associated Poisson ratio is often close to, but not equal to 0.5. It hence seems reasonable to assume that some degree of compaction, however small, may well take place. Using this approach and using a correction factor b (damping factor) of 0.03, equation (8) fits well with the available data (figures 8a and 8b). By virtue of being essentially equivalent, this obviously also applies to (7).

The average surface heave as a fraction of the measured lateral soil displacements of the measuring points up to 20 m away from the pile axis is around 0.85. Beyond that, measured values are very small, with random noise precluding any further meaningful analyses. Note that the observed average value of 0.85 for the ratio of vertical heave to horizontal displacement is in line with the ratio using SSPM theory, which decreases from 1 to 0.65 at a distance of 20 m away from the pile axis. Noting that the heave function f_v as per Chong (2013) essentially designates the ratio between heave and lateral displacement, the value of 0.85 can be considered as the empirical determined heave function,

and the correction factor b subsequently calculated. Using the pile length of 45 m and radius of 0.3, this factor is calculated as 0.019. As the correction factor according to Chong only considers volume lost to heave, the excess of 0.011 is attributed to soil compressibility.

The extensometer data are less straightforward to interpret. Using SSPM theory to predict the vertical soil movements for each extensometer and every pile installed and adding the resultant movement, it shows that the shallow strain path method overpredicts the aggregate vertical soil movements for all extensometers but the ones located at a depth of 20 m. Noting that the soil at 20 m is the only layer that resembles a homogenous, undrained soil, this seems suggest that the vertical displacement of mixed soils is in general accordance with SSPM theory, but dampened due to some degree of compressibility. Therefor and in analogy to (7) and (8), a similar damper function is introduced to reflect compressibility:

$$\delta_{r,z} = \delta_{r,z\,(\mathrm{SSPM})} \cdot (1-b)^r \qquad (9)$$

where $\delta_{r,z\,(\mathrm{SSPM})}$ denotes the vertical displacement at radius r and depth z as per SSPM. The corrective damper b was subsequently varied to match the measured data. Table 3 presents the associated best match values for damping, and figures 10a and 10b show the between match between measured and calculated values.

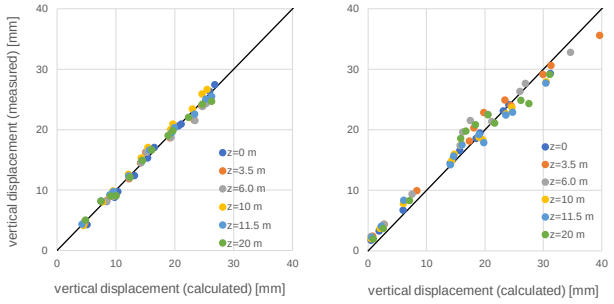

Fig. 10a and 10b. Comparison of the cumulated calculated and measured vertical displacements at various depths for line A and B after the construction of 12 piles.

Table 3. Best match values for damping b

line	extensometer at depth z					
	0.0 m	3.5 m	6.0 m	10.0 m	11.5 m	20.0 m
A	0.027	0.040	0.040	0.030	0.022	0.00
B	0.032	0.010	0.030	0.030	0.022	0.00

Note that the average value for damping at the ground surface is 0.03. Values for the extensometers located at a depth of 6, 10, 11.5 and 20 vary only minimally or not at all. These values seem layer-specific and plausible with respect to the soil layers. A damping value of 0, as determined for both extensometers at 20 m, denotes ideal incompressible behavior. Values above zero reflect some degree of compressibility, with higher values reflecting a larger compressibility. Note that the vertical displacements of both extensometers located at 6 m depth, located in a gravelly sand, still generally comply with the shallow strain path method, albeit dampened. The value of b for the extensometer located at a depth of 3.5 m differ significantly. This is attributed to natural soil variability: as per cone penetration test, the extensometer should be located in a organic clay, just below a layer of loose sand. Based on other CPTs made on site, this sand layer is known to vary significantly, locally increasing in thick and relative density while being completely absent at others. Hence, it is believed that at line A, this extensometer happens to be anchored in sand.

The extensometers were logged quasi-continuous as opposed to the total station and level measurements. The settlement of the extensometers in between piling is readily recognizable, and correlates with a decrease in excess porewater pressure. Settlement occurs in a log-linear fashion, as does the decrease of the excess pore water pressure measurements, suggesting that the time-dependent reconsolidation is controlled by the drainage of excess pore water pressure. A first-order approximation can be written as

$$\delta_{z,t} = \delta_{z,0} - \frac{\delta_{z,end} - \delta_{z,0}}{log(t_{end}) - log(t_0)} \cdot \log t \qquad (10)$$

with $\delta_{z,t}$ denoting the vertical soil displacement at time t and radius r, and $\delta_{z,0}$ and $\delta_{z,end}$ the vertical displacement immediately after pile installation at time t_0 and at the end of reconsolidation at t_{end}, respectively. Using a minimum of two site observations for soil heave, the reconsolidation can then be described.

10 CONCLUSIONS

Fundex-type full displacement piles can be constructed with diameters up to 700 mm and a length of 45 m. The axial capacity is accordingly: during a series of 4 axial maintained static load test on full displacement piles with a diameter of 600 and 700 mm, respectively, the maximum loads applied were around 6800 kN (600 mm) and 7800 kN (700 mm), respectively. None of the piles met the European or Swiss requirements for failure. Such high axial loads provide new possibilities for economic pile design. The load-deformation curve at the pile head predicted during preliminary design correlate reasonably with the measured pile head displacement. The largest deviation occurred at test pile P4. It is possible that the construction order influences the response at the pile head, as the pile constructed last is not subject to the effects of vertical soil displacement stemming from the installation of later piles.

The strain measurements prior to testing show that significant strains are already present prior to testing. Some of these strains are irreversible and believed to be introduced during the first ca. 12 hours after concrete casting. Residual loads must be considered during analyses of static pile load test results.

The lateral and vertical soil displacements measured during the installation of the reaction and test piles are in

general accordance with the shallow strain path method, but predictions tens to overestimate these displacements in mixed soils and gravelly sand. The SSPM method can be modified by introducing a damping function to allow for soil compressibility. Using this approach, damping values can be derived for separate soil layers. Barring measurements, tentative values of 0.025 ± 0.005 for mixed, primarily silty soils and 0.035 ± 0.005 for medium dense to dense sands appear reasonable. Higher values appear reasonable for looser sands.

REFERENCES

1) Bamforth, P, Chisholm, D., Gibbs, J. and Harrison, T. (2008), The Concrete Centre, Properties of Concrete for use in Eurocode 2

2) Baligh, M. M. (1985): Strain path method, *Journal of Geotechnical Engineering* 111.9, 1108–1136.

3) Carter, J.P., Randolph, M.F. and Wroth, C.P. (1979): Stress and Pore Pressure Changes in Clay during and after the Expansion of a Cylindrical Cavity, *International Journal for Numerical and Analytical Methods in Geomechanics*, Vol. 3, pp 305-322

4) Chong, M. K. (2013): Soil Movements Due to Displacement Pile Driving, International Conference on Case Histories in Geotechnical Engineering, 30.

5) Cooke, R. W. and Price, G. (1973): Strain and displacements around friction piles, *Proceedings of the eighth International. Conference on Soil Mechanics and Foundation Engineering*, Moscow, 2, No. 1, 53-60.

6) Eslami, A. and Fellenius, B.H. (1997): Pile capacity by direct CPT and CPTu methods applied to 102 case histories. *Canadian Geotechnical. Journal,* 34 (6), 880–898.

7) Fellenius, B. H. (2022): Basics of Foundation Design, Electronic Edition, January 2022

8) Hagerty, D.J. and Peck, R.B. (1971): Heave and Lateral Movements due to Pile Driving, *Journal of the Soil Mechanics and Foundation Division*, ASCE, Vol. 97, No. 11, pp 1513-1532.

9) Johnson, K. R. (2016): Advancements in Thermal Integrity Profiling Data Analysis, Ph. D. thesis, University of South Florida

10) Ni, Q., Hird, C.C. and Guymer, I. (2010): Physical modelling of pile penetration in clay using transparent soil and particle image velocimetry, *Géotechnique* 60(2) 121-132.

11) Niazi, F. W. and Mayne, P. W. (2016): CPTu-based enhanced UniCone method for pile capacity, *Engineering Geology* 212, 21–34

12) Poulos, H. G. (1994): Effect of pile driving on adjacent piles in clay, Canadian Geotechnical Journal, Ottawa, 31(6), 856–867.

13) Randolph, M.F., Carter, J.P. and Wroth, C.P. (1979).: Driven Piles in Clay – the Effects of Installation and Subsequent Consolidation, *Géotechnique* Vol. 29, No. 4, pp 361-393

14) Randolph M.F., Steenfelt J.S., and Wroth C.P. (1979): The effect of pile type on design parameters for driven piles, Design Parameters in Geotechnical Engineering, BGS, London, vol2, pp.107-114

15) Sagaseta C., Whittle A.J., and Santagata M. (1997): Deformation Analysis of shallow penetration in clay, *International Journal for numerical and analytical methods in Geomechanics*, vol 21, 687-719

16) Sagaseta C. and Whittle A.J. (2001): Prediction of Ground movements due to pile driving in clay, *Journal of Geotechnical and Geoenvironmental engineering*, Jan 2001, p55-66

17) Tuenter, H. J. and Rozálen Garcia, V. (2017): Die Anwendung der revidierten UniCone Methode zur Vorhersage des Last-Setzungsverhaltens von Ortbeton-Verdrängungspfählen, Mitteilung des Instituts für Grundbau und Bodenmechanik Technische Universität Braunschweig, Heft Nr. 102, Pfahl - Symposium 2017, 481-494

18) Vytiniotis, A., Casey, B. and Sykora, D. W. (2018): Lateral Soil Movements Due to Pile Driving: A Case Study in Soft Clays, International Foundation Congress and Equipment Expo 2018, Orlando, Florida, March 5–10, 2018.